International Journal of Engineering and Applied Science October 6 University
https://ijeasou.journals.ekb.eg/
Online ISSN 3009-6448
Volume (2),Issue(1)
January 2025, pp:80-90

Improvement The Frequency Response for Interconnected Area Power System Using Artificial Intelligence Techniques

Mohamed Abdelkareem[1], M. A. Abdelghany[2*], Diana Refaat Henry[2], Shorouk Ossama Ibrahim[2]

[1] Department of Astronomy, National Research Institute of Astronomy and Geophysics, Cairo, Egypt
[2] Department of Electrical Engineering, Faculty of Engineering, October 6 University, 6th of October City, 12585, Giza, Egypt.
* Corresponding author's email: m.a.abdelghany.eng@o6u.edu.eg

https://doi.org/10.21608/ijeasou.2025.349260.1038

Received:31 December 2024
Accepted:12 January 2025
Published:13 January 2025

Abstract – This study introduces an updated recommended design of intelligent Load Frequency Controllers (LFCs) for an off-grid 2-area Hybrid Microgrid. Harris Hawk Optimization (HHO) is used to create intelligent fine tuned Proportional-Integral-Derivative (PID) as well as Fractional-Order PID (FOPID) controllers. The envisioned HHO method's performance is validated on a 2-area off-grid Hybrid Micro-Grid (HMG) HMG in the presence of various renewable energy resources and diverse types of energy storage systems (ESSs) under assortment of case studies a variety of scenarios, including fluctuations in load, solar irradiance, and speed of wind, using realistic measurements. The prescribed goal function and control gains are the integral-time sum of absolute deviancies and controller settings, respectively. The system's dynamic reaction and simulation findings demonstrate that the recommended HHO based FOPID LFCs are successful in dipping frequency and tie-line power signal variations in a short time. For additional validations, simulation results are compared to genetic algorithms to determine the factors of the suggested controllers to find out the parameters of the implemented controllers.

Keywords: Load Frequency Controllers, Hybrid Microgrid, Harris Hawk Optimization, Fractional Order PID controllers, Energy Storage Systems.

I. Introduction

Hybrid microgrid featuring different forms of micro renewable resources coupled with some types of energy storage systems (ESSs) has been a major concern for researchers and companies in recent years[1]. The relevance of ESSs is clarified providing the power produced by wind and solar systems is oscillating in random manner and intermittent. battery storage, supermagnetic energy storage and supercapacitors are being considered in [2] as a types of ESSs. Natural fluctuations deviations in sun irradiations, wind velocity and load disruptions may result in significant and serious power oscillations [3]. Such variations of power output from all the renewable sources could stimulate a significant issue with system frequency as well as voltage oscillations. Load frequency controller (LFC)'s primary role is to resolve this fluctuation besides authorize that systems' dynamic behaviour is in an endurable tolerance [4]. A necessity for effective and productive LFCs is therefore crucial, particularly when the electric grid is operating in an isolated state.

Papers in literature proposed LFCs for HMG using traditional approaches and numerous artificially intelligent related techniques. Traditional PI controllers[5], classic Ziegler_ and Nichols LFCs based on Ziegler_Nichols' method [6], as well as H-infinity constructed controllers were introduced as conventional models types of LFCs [7]. Moreover, artificial intelligence techniques as well as swarm approaches were used to optimize the responses of systems like artificial neural_networks[9], fuzzy_controllers[10], particle swarm optimisation [11], biogeography optimisation technique [12], harmony search algorithm [13]. Furthermore, wide ranging technical assessments and detailes are discussed and described in [14–16].

The Harris Hawks optimization (HHO) method is used to fine tune the settings for the PID and FOPID controllers optimally, which is the work's main originality. Introducing the Harris Hawks Optimization (HHO) approach to optimize the parameter values for the PID and FOPID controllers, is the research work's main objective. The key feature for HHO is the cooperating disposition and manner of pursuing Harris' hawks in the natural world, also known as the surprise pounce. Throughout this brilliant strategic

technique, numerous hawks swoop on a prey in a continual endeavor to surprise it from various directions. Harris hawks may distribute a number of hunting paradigms based on the dynamic nature of all settings and their prey's escape tendencies.

The stimuls of this paper is to demonstrate besides disclose the strengthness of the based HHO PID and FOPID controllers in an off grid HMG under exceedingly random conditions. This article addresses intelligent LFCs' optimum scheme in addition best fine-tuning to enhance the response of system with two area standalone HMG. HHO is used for the determination of optimum LFC parameters HHO is employed to find out the optimal LFCs' settings. The proposed HHO-based approach is applied on an integrated HMG that involves hybrid wind/diesel/solar systems with distincit types having ESSs. Maximum power point tracking operation approachs of wind turbines' generators and photovoltaic generating arrays make both of them not contributing in frequency regulation in this study. With subsequent discussion and analysis, frequent consequences are prearranged for dynamic simulation to reveal the effectiveness of the suggested control system. Via MATLAB_SIMULINK software the proposed model of studied HMG involving ESSs is simulated and established. Assessments with Genatic algorithm (GA) are concidered to authenticate HHO recommended methodology in different cases and operating conditions.

II. Off grid Hybrid Microgrid model

The proposed two-area HMG simulation model for this research is validated in Fig. 1. The area-1 consisted mainly of a wind turbine generator (WTG), diesel engine generator (DEG), and super conducting magnetic energy storage (SMES) system. By comparison, area-2 includes a solar photovoltaic (PV) array, a DEG, as well as a battery energy stotage (BES) system. The major sources for meeting power demands are WTG's and PV's. Both can be worked under irregular circumstances owing to fluctuations of wind speed and solar radiation in nature. The DEGs have been used as a back - up power supplies for load responses. Nevertheless, the SMES and BES components are being used for system requirements of short-term backup operations. The presented hybrid wind-diesel-PV system is really very reliable as it acts as a cushion to take account of variations in wind speed and sun radiations and would continuously sustain an average power equal to the reference point. The enlargement of such hyprid power generation system is expected to cover the vastly increased power demands for such an isolated community. The feature of the introduced control scheme for this work would be that the controllers of each DEGs and ESSs are used for damp frequency as well as tie line power deviation and to significantly reduce steady-state error throughout frequency and tie line power in a shortened selting time. Furthermore, the stimulation of maximum power tracking of PVs and Wind turbines, specifically with continuous variations in solar radiations and wind speed, is applicable. The characteristics of the various components of the studied HMG are exemplified as follows through the next sub sections.

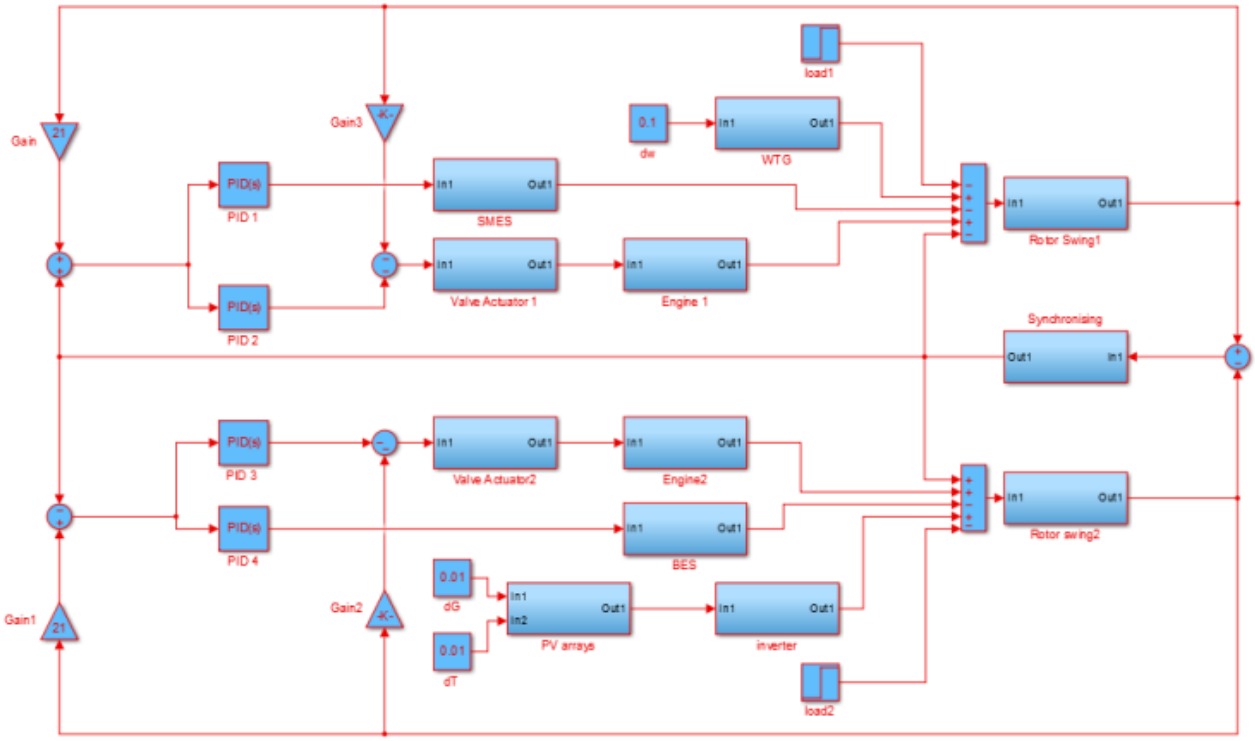

Fig. 1 The suggested model for isolated 2 area system of HMG.

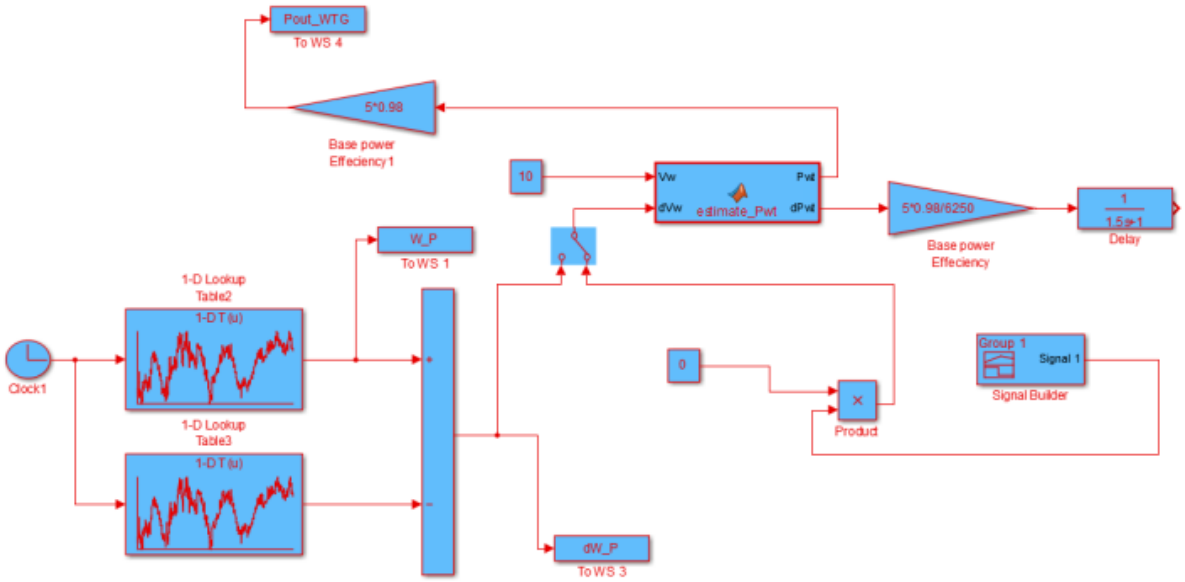

Fig. 2 WTG system model.

A. wind turbine Generation system

The generated power by the P_{WT} turbine is described by the expression specified in (1) [18], and its efficiency coefficient[19] is calculated analytically using manifestations in (2) and (3). C_P is typically operated at low to medium wind speeds to allow the turbine to function optimally.

$$P_{WT} = \frac{1}{2} C_P \rho A v_\omega^3 \tag{1}$$

$$C_P = C_1\left(\frac{c_2}{\lambda_r} - c_3\beta - c_4\right)e^{(-(c_5/\lambda_r))} + c_6\lambda_r \tag{2}$$

$$\lambda = \frac{\omega_t r}{v_w} \tag{3}$$

The WT generation simulink model is showin in Fig.2. It's noteworthy that C_P is a very manufacturer-specific parameter. That research will involve the GAMESA wind turbine, which was erected in Egypt's Zafarana district[17]. The data sheet for that wind turbine is shown in the appendix. The primary goal is to operate the wind turbine at peak efficiency. The mean power capacity of the GEMESA wind turbine may be computed using the parameters specified in (4) once its curve fitting is completed. However, enhancements in the GEMESA ΔP_w wind power output can be projected as shown in (5).

$$P_w = \begin{cases} 0 & v_w \le v_{cut-in} \,\&\, v_w \ge v_{cut-out} \\ P_r & v_r \le v_w \le v_{cut-out} \\ 0.001312v_w^6 - 0.04603v_w^5 + 0.3314v_w^4 - 3.687v_w^3 & else \\ 51.1v_w^2 + 2.33v + 366 & \end{cases} \tag{4}$$

$$\Delta P_W = \begin{cases} 0 & v_w \le v_{cut-in} \,\&\, v_w \ge v_{cut-out} \\ 0 & v_r \le v_w \le v_{cut-out} \\ [0.007872v_w^5 + 0.23014v_w^4 - 1.3256v_w^3 & else \\ 11.061v_w^2 + 102.2v + 2.33]\Delta v_w & \end{cases} \tag{5}$$

B. Solar PV Generation system

It is vital to remember that the photovoltaic solar production Psolar is mostly determined by the amount of sunshine and the temperature. Severely, if the air temperature remains fixed at 25° C, Psolar fluctuates only in a linear fashion with G. MPPT (maximum_power_point_tracking) techniqes are commonly used in solar power generation to improve the overall power efficiency. [20]. (7) describes how changes in sunshine and temperature affect solar power generation (ΔP_{solar}). During this study, 98 percent of the effective MPPT approaches were deemed to be proficient. Every array is specified with a capacity rating of 200 kW within the STC, with five connected on a parallel basis for producing 1000 kW at the STC (data sheet in appendix) Fig.3 depicts the implemented PV generation simulink system.

$$P_{solar} = P_{PV}\frac{G}{G_{STC}}(1 + K_t[T_a + 0.0256G - T_{STC}])\eta_{MPPT} \tag{6}$$

$$\Delta P_{solar} = \frac{P_{PV}}{G_{STC}}(\Delta G + K_t[\Delta G T_a + G\Delta T_a + 0.05126G\Delta G - T_{STC}\Delta G])\eta_{MPPT} \tag{7}$$

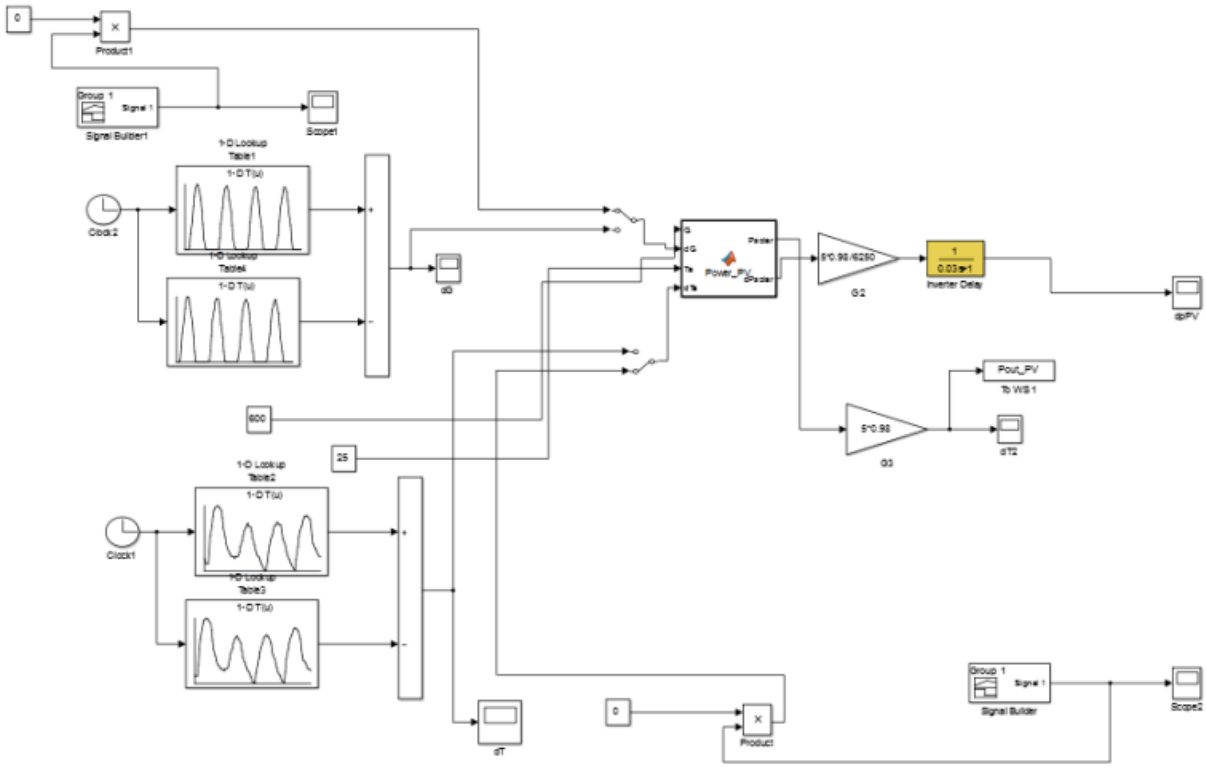

Fig. 3 Schematic diagram of PV generation system.

C. Batery energy storage system

The proposed method employs the model of Redox Flow Battery (RFB), which is a type of electrochemical recharging energy storage. The RFB is an electrochemical recharging energy storage device that has increased capacity, rapid response, and a reduced issue of backup self-depletion. During the chemical reactions phases, the BES stores DC electric energy while also providing a converter and an inverter to exchange AC electricity. The fundamental notions of such battery's structures are properly illustrated in [21]. Figure 4 shows a generic schematic for RFB. During typical load demands, batteries charge then promptly return energy to the the network. A dual converter converts DC to AC or AC to DC. RFB offers an efficient response to the issue of LFC.

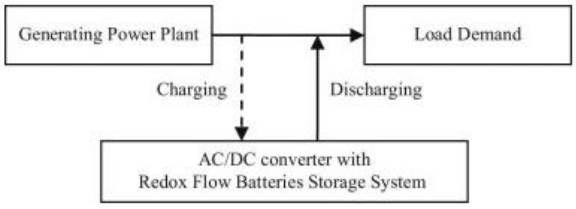

Fig. 4 Block diagram of RFB system

D. Superconducting Magnitic Energy Storage System

The electric energy is stored (E) in the coil in the form of a magnetization fields, which is provided via (8). Even so, the corresponding SMES' power (P) is estimated as revealed in (9)[22]. Figure 5 shows a SMES detailed schematic representation.

$$E = \frac{1}{2} LI^2 \qquad (8)$$

$$P = \frac{\partial E}{\partial t} = LI\frac{\partial I}{\partial t} = VI \qquad (9)$$

wherein L represents the superconductivity of coil inductance, I is the electric current flowing via the coil, while V indicates the electrical voltage throughout the coil.

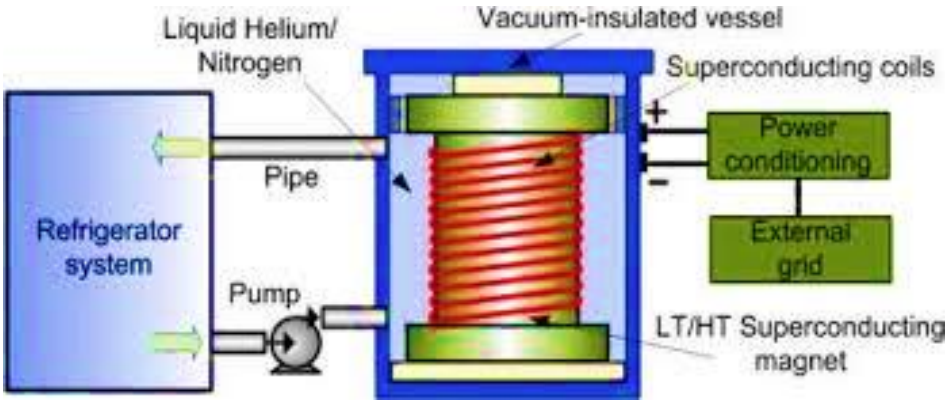

Fig. 5 SMES schematic diagram.

E. Desil engine generation system

Both wind and solar energy sources are irregular owing to changing atmospheric conditions, making PV and wind power output uncertain. In independent or freestanding hybrid energy systems, energy of renewables are normally paired through DEGs to deliver steady demand to independently customers. DEG sets of synchronous electrical generators and renewable sources of energy operate in tandem to meet demand for energy over such a tiny distribution network.

The diesel-powered power generating unit has a speed governor that controls the diesel engine's output power. Figure 6 depicts the basic block representation model of the diesel powered generator as well as its governor of speed system[23]. The unit primarily comprised of a speed drop control has a single droop (R), a valve_actuator, as well a diesel motor. Delay of 1st order is utilized to reflect the actuators for valves and diesel engine, as well as the time constants T_e and T_v. U_{dg} is the LFC controlling signal, Δf is the frequency deviation, X_g is the pump positional increment, and P_{dg} is the change in the diesel engine's mechanical power. Each DEG has a rating of 500 kVA.

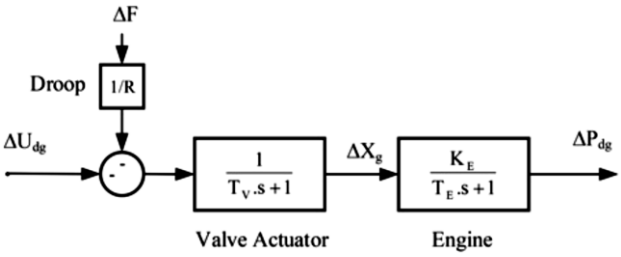

Fig. 6 Block diagram of DEG system

Typically, DEG's responsiveness to load changes is restricted across energy regulation systems. DEGs also offer near-instant demand response capability, and they can manage massive block loads tends to 100% of engine nominal capacity in single step[24]. In normal operation, the output of the DEG is managed to avoid overloading situations; however, in the event of a heavy load demand, in cooperation ESS and DEG produce the power to meet this need.

It needs to be noted that the electrical demand is considered to be sufficiently high to allow for maximum power extraction from both the wind turbine and the PV. For this situation, there shall be no capacity to reserve for the wind powered generators or the PV to contribute to prime frequency regulation, therefore the frequency will be managed by diesel generators and assisted by transient energy transfer from energy storage devices[25]. As a result, this report includes a basic first order transfer function that ignores any nonlinearity.

Table 1 shows the 2 area HMG subsystems transfer functions, together with the usual parameter values utilized in this study.

TABLE I
The Transfer functions of components in the two area HMG system

Subsystem	Transfer Function	Values
WTG	$\frac{K_W}{T_W S+1}$	$K_W=1$ $T_W=1.5$
PV	$\frac{K_{pv}}{T_{pv} S+1}$	$K_{pv}=1$ $T_{pv}=0.03$
SMES	$\frac{K_L}{T_L S+1}$	$K_L=0.98$ $T_L=0.03$
Battery System	$\frac{K_B}{T_B S+1}$	$K_B=1.8$ $T_B=0$
Valve_ Actuator1,2	$\frac{1}{T_v S+1}$	$T_v=0.05$
Diesel_Engine1,2	$\frac{K_E}{T_E S+1}$	$K_E=1$ $T_E=0.5$
Rotor Swing$_1$	$\frac{K_{p1}}{T_{p1} S+1}$	$K_{p1}=1$ $T_{p1}=3$
Rotor Swing$_2$	$\frac{K_{p2}}{T_{p2} S+1}$	$K_{p2}=1$ $T_{p2}=3$
Synchronising	$\frac{T_{12}}{S}$	$T_{12}=4.398$
Frequency biases	B_1,B_2	B_1=21 B_2=21
Droops	R_1,R_2	R_1=0.05 R_2=0.05

V. Harris hawk Optimization Algorithm

Harris' hawk is a renowned raptor of prey that lives in the southern part of Arizona, USA. Through the non breeding

time of the year, these intelligent birds may host meal parties for a large group. Hawks periodically conduct a "leapfrog" maneuver all around the target spot, rejoining and splitting multiple times to aggressively look for the concealed prey, which is generally a rabbit. Harris's hawk can be recognized by its unique collaborative foraging behaviors with relatives living in a similar stable group, whereas other raptors typically assault to find and capture a target on their own.They are regarded as really forthcoming predators within the raptor world. The major approach for capturing a target is "surprise pounce", commonly referred to as "seven kills" technique. They recognize their closest relatives and try to anticipate their movements throughout the attack. Whenever the best hawk (the leader) kneels at the target and becomes disoriented, one of the group's members will take up the hunt. Harris' hawk may pursue the discovered rabbit until weariness, increasing its susceptibility. Most prominent and knowledgeable, typically the strongest, quickly captures the weary rabbit and trades it to other party leaders, rendering the bunny powerless [26]. Figure 7 shows a generalized flow chart for HHO.

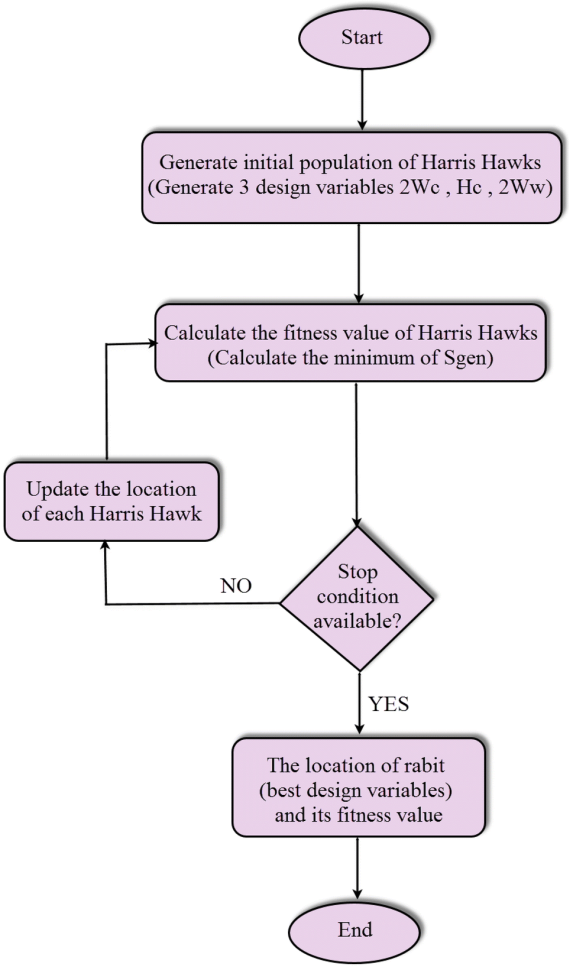

Fig. 7 General HHO flow chart

Fractional order PID controller

FOPID controller was introduced by Igor Podlubny [27]. It would be supplement of the traditional PID controller type where a certain fractional μ and λ values are available. Figure 8 displays block diagram of the PID fractional-order system. The predscribed integral differential-equation describing the controllers' processing of a fractional-order PID controller is given as follows:

$$u(t) = K_P e(t) + K_I D^{-\lambda} e(t) + K_D D^{\mu} e(t) \qquad (10)$$

In addition, the FOPID controller transfer-function in the S-domain can be discribed as follows:

$$u(s) = (K_P + \frac{K_I}{s^{\lambda}} + K_D s^{\mu}) e(s) \qquad (11)$$

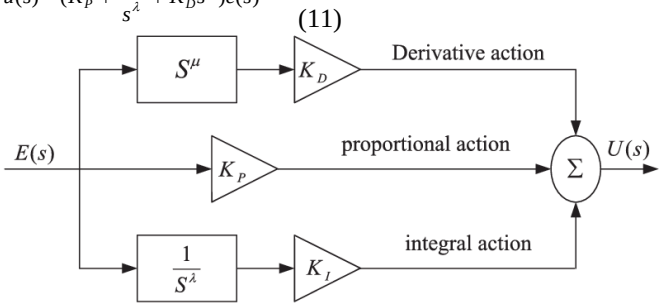

Fig. 8 FOPID controller block diagram

VI. Intelligent optimized Controllers

Frequency controllers optimum tuned settings are obtained by proactively taking into consideration differences in frequency ranges besides tie line strength. Integral Timed Weighted Absolute Error (ITAE) is identified such as the function of fitness (FF) to be diminished in (12) refer (12) owing to its several advantages in the improving mechanism of the system time of settling. Identification of the objective functions is indeed the major factor for any real system enhancement time-response. ITAE criteria obviously has the advantage of creating lesser overshoots and oscillations vacillations than the integral absolute error or integral square error (IAE or ISE) metrics [28-29]. Accordingly, the ITAE test is employed to fine-tune the controllers. Related to the gains' limitations which are described throughout the next formula:

$$K^k_{P,I,D_{\min}} \le K^k_{P,I,D} \le K^k_{P,I,D_{\max}}$$

The data input for every controller is basically the variance amongst B • ΔF as well as the ΔP error for the 2 regions. LFCs remain developed to minimize deviation, resulting in lower ΔF and ΔP. The suggested HMG model, illustrated in Fig. 1, uses two PID control units for each DEG (PID2 & PID3), also it includes PID controllers for the each ESS (PID 1 intended to SMES; and PID4 to BES).

Twelve control variables define all gains for PID controllers. HHO is used to minimize FF abovementioned and to observe with all relevant inequalities restrictions. It is value noting that FCs were being designed off-line at the planning stage and only placed into online practice to fine-tune the operation of the grid system via load disturbances [30].

Likewise, in communal practice FCs using PID are manipulated for various load shift scenario values. Subsequently, design level of the PID that is dealt with as a planning process, is carried out off line using the recommended HHO procedure before all the FCs are placed into service.

$$ITAE = \int_0^T t(|\Delta F_1| + |\Delta F_2| + |\Delta P_{tie}|)dt \quad (12)$$

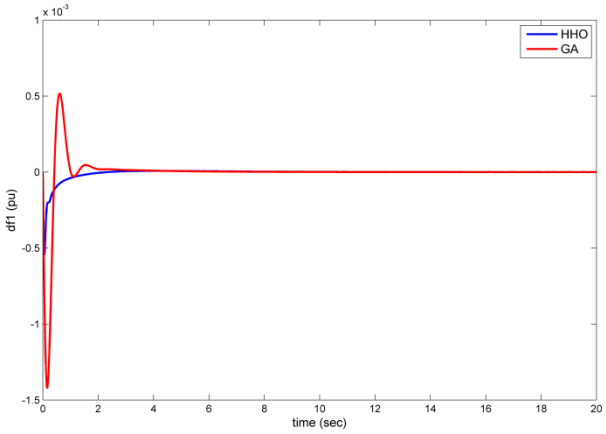

Fig. 9 Deviation for frequency in area (1) of case_ 1.

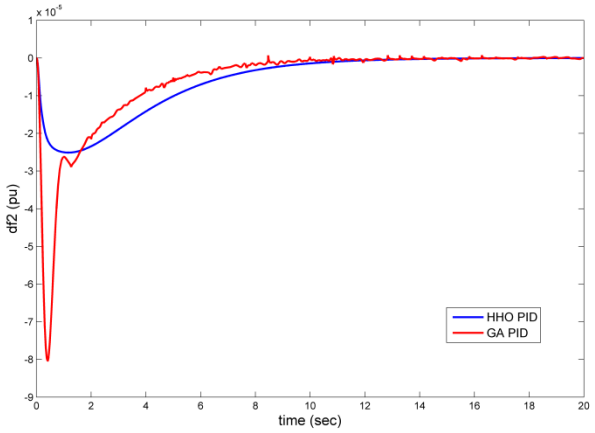

Fig. 10 Deviation for frequency in area (2)of case _1.

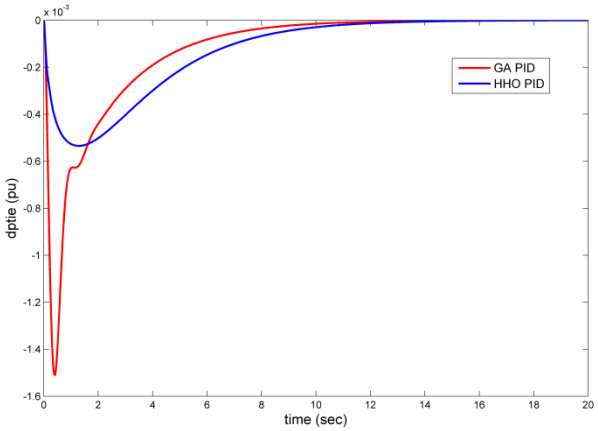

Fig. 11 deviation for tie_line power of case_1.

VII. results of Simulaton

The viability of the suggested HHO-based LFCs within a 2_ area HMG with ESSs will be investigated here in isolated operation. The HMG model is linearized to minimize sophistication while still providing reasonable approximations. As a result, the model's subsystems are condensed into linear 1st-order low-pass lag transfer functions. The designated system model as well as simulation are performed using the framework of MATLAB_SIMULINK. The acceptable controller variables for the HHO suggested approach are shown in the appendix, and they were collected from several tests. Following a definitive trial and error, the approved upper and lower boundaries of controller's parameters are selected from 0 to 5. The next subsections provide an analysis and illustration of the isolated two area HMG under various operating conditions and load disturbances. Numerous situations are examined in our current study in the manner described below:

Case _1:

Here, the av. temperature is 25 °C, the average wind velocity is 10 m/s, and sun irradiance is 600 W/m^2 (ΔV_w, ΔG, and ΔT_a are all exactly zero). At t = 0, area-1 is further exposed to a +5% load step variation. Attempts and optimum values of all parameters assessed using GA PID have been compared with the HHO PID and proved in Table 2 and Table 3. The time-domain results from simulation for ΔF_1, ΔF_2, and ΔP_{tie} are shown in Fig. 5. The optimal minimum value of ITAE utilizing HHO is 5.84756×10^{-3} out of 50 consecutive consecutive runs. Even after the confirmation of the HHO-based conclusions, the GA is still a powerful, established method that many scholars are aware of without having to review annotations.

TABLE 2
Parameters of GA optimized PID controllers

Variable	PID_1	PID_2	PID_3	PID_4
K_p	0.0067	1.2006	2.2003	2.4986
K_i	4.8848	4.9648	1.5984	4.1875
K_d	4.1558	2.5998	2.4985	1.3964

TABLE 3
Parameters of HHO optimized PID controllers

Variable	PID_1	PID_2	PID_3	PID_4
K_p	0.982	1.64158	2.2152	4.3216
K_i	8.00258	7.19875	2.3647	8.71489
K_d	4.4913	3.6438	3.9215	2.9631

The HHO is stable in addition able to provide PID settings that are extremely close to the global optimal solution for each check. By using the PID gains generated by HHO and GA, it is evident that the time domain response signatures coincide to some extent. It is clear from using the PID gains obtaind by HHO as well GA that there is some overlap between the time domain response signatures.

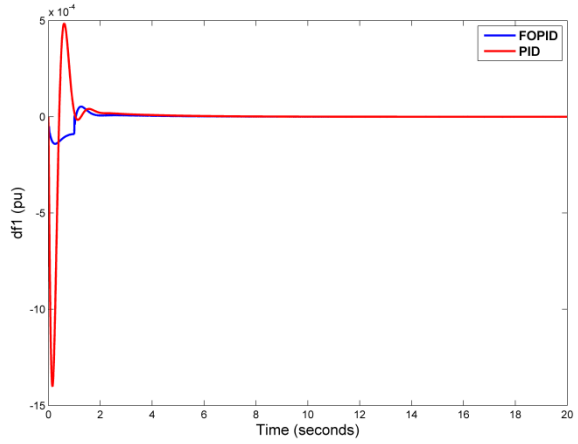

Fig. 12 Area(1) frequency deviation of case 1.

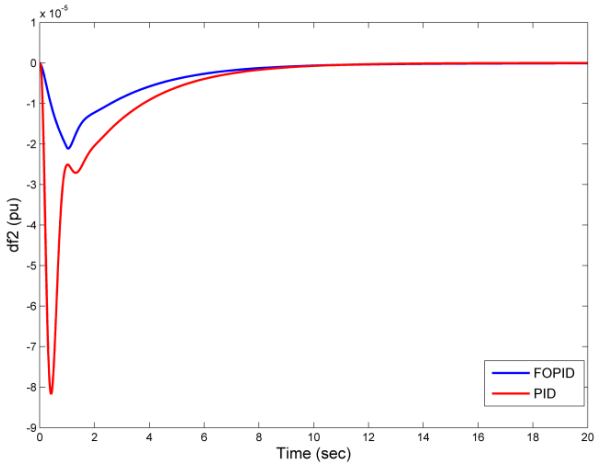

Fig. 13 Area(2) frequency deviation of case 1.

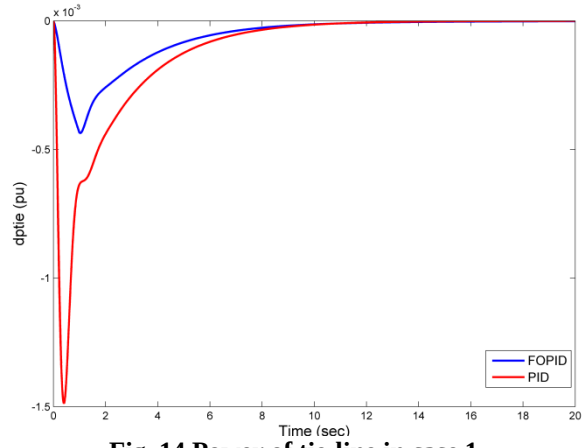

Fig. 14 Power of tie-line in case 1.

Case_ 2:

This case is where a variation in wind speed develops. At t=0.01s, the wind speed tends to increase from its starting setting of 15 m/s to 17 m/s. In this instance, adding a load to area-1 by +5% step at t = 0 causes the wind speed to abruptly increase starting 10 upto 12 m/s by t=10 s and abruptly decrease from 12 to 10 m/s at t = 15 s, even though there is no change in the ambient temperature or sun radiation (Δv_w = ±2 m/s, ΔT_a = 0, as well ΔG = 0). Furthermore, it is presumed that, while maintaining ΔG = 0 and ΔT_a = 0, a noticeably greater wind speed disruption with Δv_w = ±4 m/s is anticipated at t = 10 and 15 s. Signal variations under abrupt increases in Δv_w = ±2 m / s and Δv_w = ±4 m / s, correspondingly, are shown in Figs. 12,13 and 14. The optimal values and system response performance parameters for the settling time T_S (± 2 criteria), maximum positive overshoot, and maximum negative undershoot are also listed in Table 4 and table 5 with respect to the developed HHO-based FOPID LFCs consequently.

TABLE 4
Parameters of HHO optimized FOPID controllers

Variable	FOPID1	FOPID2	FOPID3	FOPID4
K_p	0.0148	1.1972	2.0985	2.8111
K_i	4.6472	4.9996	1.7927	4.1687
K_d	4.0024	2.5456	1.9251	1.3812
λ	0.501	0.9542	0.0801	0.1121
μ	0.0131	0.0154	0.3680	0.2101

TABLE 5
Time response values of HHO optimized controllers

	HHO PID controllers		
	Δf_1	Δf_2	Δp_{tie}
Tr (Rise_time)	4.195e-04	1.112	3.542
Over_shoot	2.342e+07	8.098e+05	6.856e+05
Under_shoot	2.415e+07	7.034e+03	0
Min._settling	-0.0013	-8.198e-05	-0.0014
Max. _settling	0.0013	7.078e-07	-2.122e-07
Peak	0.0013	8.098e-05	0.0015

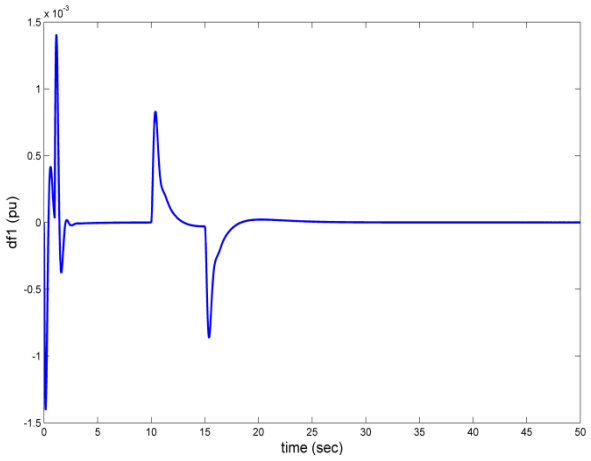

Fig. 15 Area(1) frequency deviation of case 2.

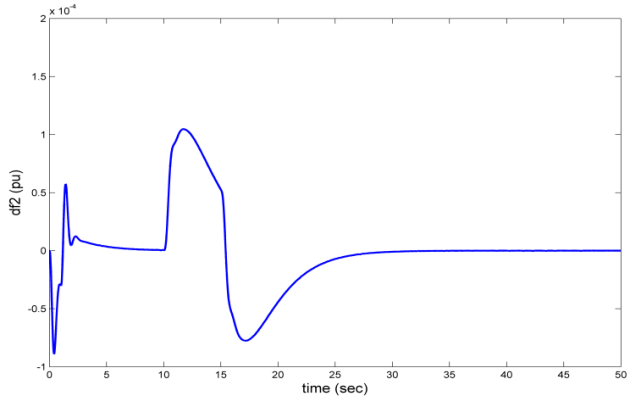

Fig. 16 Area(2) frequency deviation of case 2.

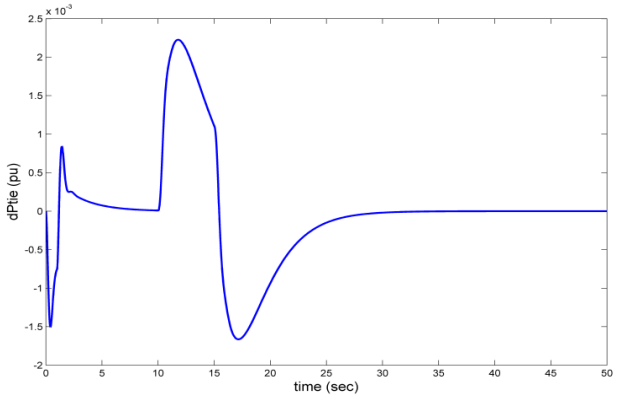

Fig. 17 Power of tie-line in case 2.

Case_ 3:

This consequence involves adding a 5% stepped load to area (1) at t = 0 besides abruptly reducing solar irradiation by ΔG = +200 W / m2 at t = 10 s step disruption. At the same time, there is no change in wind speediness or air temperature. Fig. 8 displays the overall system's dynamic reaction. Furthermore, it is assumed that the solar radiation increases significantly from 600 to 1000 W/m^2 at t = 10 s and then abruptly decreases from 1000 to 600 W/m^2 at t = 15 s without any change in wind speed or atmospheric temperature (ΔT_a = 0, ΔG = ±400 W/m^2, and Δv_w = 0) in order to demonstrate the effective results of the proposed HHO-based LFCs. By way of previously indicated, Fig. 18,19 and 20 shows the signaling deviation signatures under abrupt fluctuations.

D. Case_ 4:

In this simulation scenario, as a realistic study, real-site estimates of wind velocity, solar irradiation, and average - temperature are assumed to be typical to Egypt's Zafarana farm of wind-turbines (on Red Sea shore 120 kilometers southly from Suez). Natural wind level, solar radiation coming in, and air temperature data were collected from Zafarana. For 4 sequential days, It is worth noting that wind speed data are taken every 10 minutes. Nonetheless, data of sun radiation and temperature are collected hourly.

Figures 11a and b show the system's dynamic reactions when a +5% load step is applied to area-1 at t = 0s. To enhance system variability, area-1 receives ±5% of the regular load disturbances depicted which vary every 30 minutes. Figures 21, 22 and 23 demonstrate the system's time-domain reactions to this randomized load adjustment.

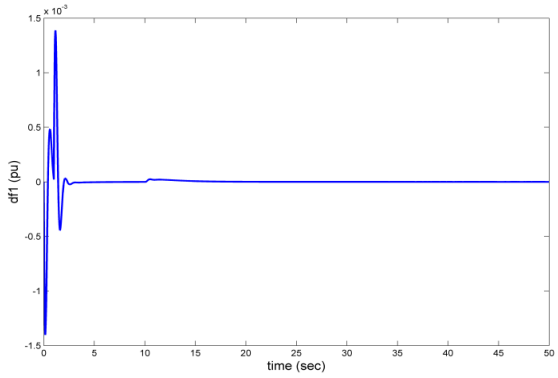

Fig. 18 Area(1) frequency deviation of case 3.

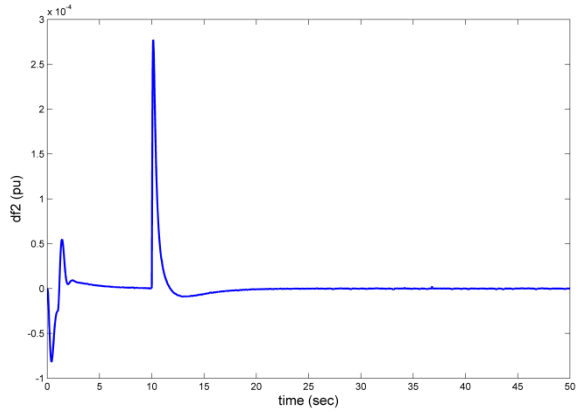

Fig. 19 Area(2) deviation for frequency of case 3.

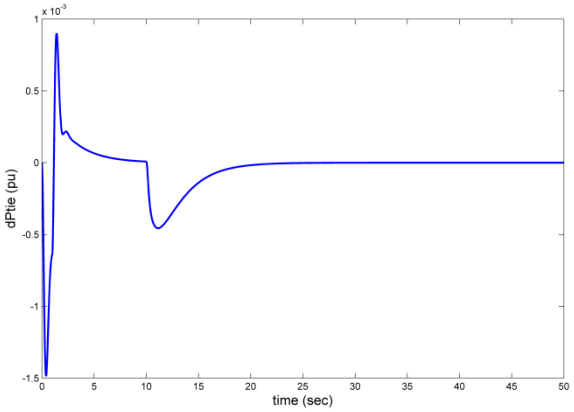

Fig. 20 Power of tie-line in case 3.

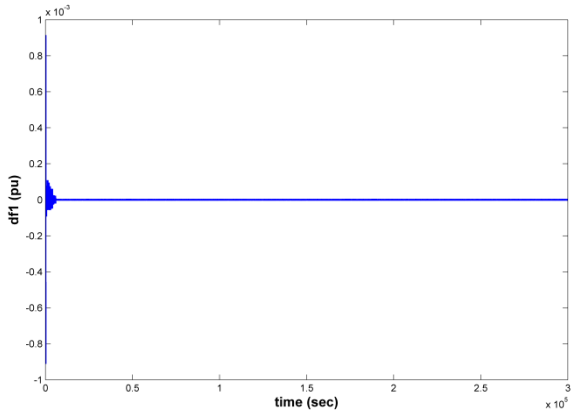

Fig. 21 Area-1 deviation for frequency of case 4.

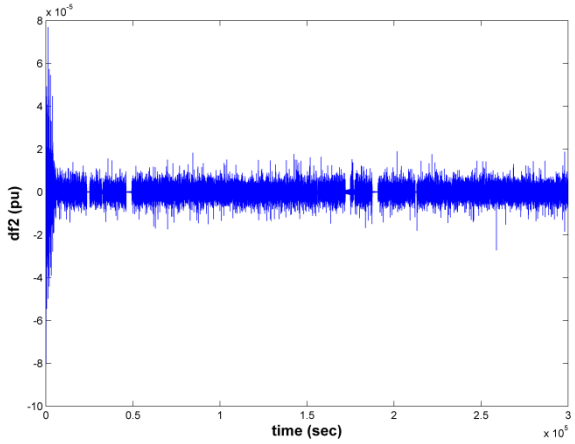

Fig. 22 Area-2 deviation for frequency of case 4.

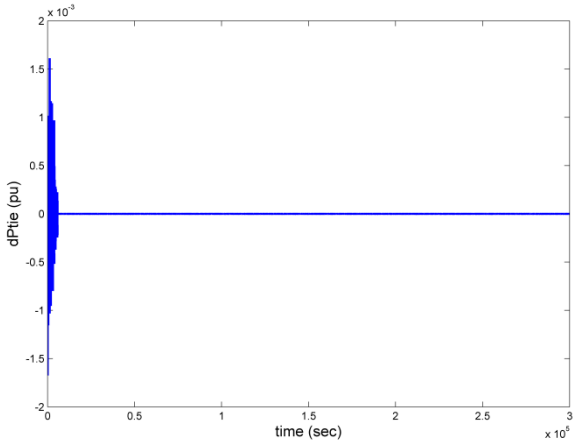

Fig. 23 Power of tie-line in case 4.

Conclusion

To enhance the system dynamic response of an isolated two-are HMG, intelligent and optimal LFCs have been proposed. GWO is used to produce the suggested controllers' ideal settings. Variability of wind-speed, perturbations of load, and daily solar radiation have all been identified and taken into account. Obtained simulations confirmed that the suggested controllers can reduce the frequency deviation signal and tie-line power signal deviations when load perturbations occur. The suggested optimization methodology's performance and excellent accuracy have been confirmed by comparison with GA. Additionally, the suggested control strategy can cope well with changes in renewable power sources [wind speed as well solar radiation]. The importance of the suggested intelligent frequency controllers is demonstrated by their quick response and reliable simulation results against variations in demand and renewable sources. Additionally, by comparing with GA, the suggested optimization methodology's high accuracy and good performance have been confirmed.

REFERENCES

[1] T. Le and B. L. Nguyen Phung, “Load Shedding in Microgrids with Consideration of Voltage Quality Improvement”, Eng. Technol. Appl. Sci. Res., vol. 11, no. 1, pp. 6680–6686, Feb. 2021.

[2] Sebastián, R. Review on Dynamic Simulation of Wind Diesel Isolated Microgrids. Energies 2021,14, 1812

[3] Sebastián, R. Review on Dynamic Simulation of Wind Diesel Isolated Microgrids. Energies 2021,14, 1812.

[4] Lastomo, D.; Setiadi, H.; Djalal, M.R. Enabling PID and SSSC for load frequency control using Particle Swarm Optimization. In Proceedings of the 2017 3rd International Conference on Science in Information Technology (ICSITech), Bandung, Indonesia, 25–26 October 2017; IEEE: New York, NY, USA; pp. 182–187.

[5] Mallesham, G., Mishra, S., Member, S., et al.: ‘Ziegler–Nichols based controller parameters tuning for load frequency control in a microgrid’. Int. Conf. on Energy, Automation, and Signal, 28–30 December 2011, Bhubaneswar, Odisha, pp. 1–8, doi: 10.1109/ICEAS.2011.6147128.

[6] Zhang, Y., Peng, C. Adaptive H∞ event-triggered load frequency control in islanded microgirds with limited spinning reserve constraints. Prot Control Mod Power Syst 8, 30 (2023). https://doi.org/10.1186/s41601-023-00303-z.

[7] Işık, M.F.; Avcil, F.; Harirchian, E.; Bülbül, M.A.; Hadzima-Nyarko, M.; Işık, E.; İzol, R.; Radu, D. A Hybrid Artificial Neural Network-Particle Swarm Optimization Algorithm Model for the Determination of Target Displacements in Mid-Rise Regular Reinforced-Concrete Buildings. Sustainability 2023, 15, 9715. https://doi.org/10.3390/su15129715.

[8] Tarkeshwar, M.V.: ‘A novel quasi-oppositional harmony search algorithm and fuzzy logic controller for frequency stabilization of an isolated hybrid power system’, Int J. Electr. Power Energy Syst., 2015, 66, pp. 247–261, doi: 10.1016/j.ijepes.2014.10.050.

[9] Aloo, Linus A., et al. "Modeling and control of a photovoltaic-wind hybrid microgrid system using GA-ANFIS." Heliyon 9.4 (2023).

[10] Pandey, S.K., Mohanty, S.R., Kishor, N., et al.: ‘Frequency regulation in hybrid power systems using particle swarm optimization and linear matrix inequalities based robust controller design’, Int J. Electr. Power Energy Syst., 2014, 63, pp. 887–900, doi: 10.1016/j.ijepes.2014.06.062.

[11] Kumar, R.H., Ushakumari, S.: ‘Biogeography-based Tuning of PID controllers for load frequency control in microgrid’. 2014 Int. Conf. on Circuit, Power and Computing Technologies [ICCPCT], Nagercoil, 20–21 March 2014, pp. 797–802, doi: 10.1109/ICCPCT.2014.7054992

[12] Peddakapu, K., et al. "Frequency stabilization in interconnected power system using bat and harmony search algorithm with coordinated controllers." Applied Soft Computing 113 (2021): 107986.

[13] El-Fergany, A.A. and El-Hameed, M.A. (2017), Efficient frequency controllers for autonomous two-area hybrid microgrid system using social-spider optimiser. IET Gener. Transm. Distrib., 11: 637-648. https://doi.org/10.1049/iet-gtd.2016.0455.

[14] Nandar, C.S.A.: ‘Robust PI control of smart controllable load frequency for frequency stabilization

of microgrid power system', Renew. Energy, 2013, 56, pp. 16–23, doi: 10.1016/j.renene.2012.10.032.

[15] R. S, S. Neelakandan, M. Prakash, B. T. Geetha, S. Mary Rexcy Asha, and M. K. Roberts, "Artificial humming bird with data science enabled stability prediction model for smart grids," Sustainable Computing: Informatics and Systems, vol. 36, p. 100821, Dec. 2022, doi: 10.1016/j.suscom.2022.100821.

[16] Çelik, E., Öztürk, N. and Houssein, E.H., 2023. Improved load frequency control of interconnected power systems using energy storage devices and a new cost function. Neural Computing and Applications, 35(1), pp.681-697.

[17] Ramos, A.F., Ahmad, I., Habibi, D. and Mahmoud, T.S., 2023. Placement and sizing of utility-size battery energy storage systems to improve the stability of weak grids. International Journal of Electrical Power & Energy Systems, 144, p.108427.

[18] Borhanazad, H., Mekhilef, S., Ganapathy, V.G., et al.: 'Optimization of micro-grid system using MOPSO', Renew. Energy, 2014, 71, pp. 295–306, doi: 10.1016/j. renene.2014.05.006.

[19] Vittal, V., Ayyanar, R.: 'Grid integration and dynamic impact of wind energy' (Springer, New York Heidelberg Dordrecht London, 2013), ISBN 978-1-4419-9322-9, Chapter 3: pp. 1–17, doi: 10.1007/978-1-4419-9323-6

[20] WINDPOWER. available at: http: //www.thewindpower.net/turbine_en_42_gamesa_g52 - 850.php (accessed on 12/Mar/2016).

[21] Sánchez-Díez, Eduardo, et al. "Redox flow batteries: Status and perspective towards sustainable stationary energy storage." Journal of Power Sources 481 (2021): 228804.

[22] Cansiz, Ahmet, et al. "Integration of a SMES–battery-based hybrid energy storage system into microgrids." Journal of Superconductivity and Novel Magnetism 31 (2018): 1449-1457.

[23] Yang, J., Zeng, Z., Tang, Y., et al.: 'Load frequency control in isolated micro-grids with electrical vehicles based on multivariable generalized predictive theory', Energies, 2015, 8, (3), pp. 2145–2164, doi: 10.3390/en8032145

[24] Generation Choices for Microgrids. Available at: http://www.elp.com/articles/print/volume 93/issue1/sections/renewables-sustainability/generation choices-formicrogrids. html (accessed on June, 2016)

[25] Ali Asghar Heidari, Seyedali Mirjalili, Hossam Faris, Ibrahim Aljarah, Majdi Mafarja, Huiling Chen, Harris hawks optimization: Algorithm and applications, Future Generation Computer Systems, Volume 97, 2019, Pages 849-872.

[26] Abdel-Basset, M.; Ding, W.; El-Shahat, D. A hybrid Harris Hawks optimization algorithm with simulated annealing for feature selection. Artif. Intell. Rev. 2021, 54, 593–637

[27] Ghany, MA Abdel, et al. "Type-2 fuzzy self-tuning of modified fractional-order PID based on Takagi–Sugeno method." Journal of Electrical Systems and Information Technology 7 (2020): 1-20

[28] Elhameed, M.A., El-Fergany, A.A.: 'Water cycle algorithm-based load frequency controller for interconnected power systems comprising non-linearity', IET Gener. Transm. Distrib., 2016, in press doi: 10.1049/iet-gtd.2016.0699.

[29] Zhaosheng, L.I.: 'The optimization design of PID controller parameters based on particle swarm optimization'. Fifth Int. Conf. on Advanced Materials and Computer Science (ICAMCS 2016), Qingdao, China, March 26-27, 2016, pp. 460–484.

[30] Sahu, R.K., Gorripotu, T.S., Panda, S.: 'A hybrid DE–PS algorithm for load frequency control under deregulated power system with UPFC and RFB', Ain Shams Eng. J., 2015, 6, pp. 893–911, doi: 10.1016/j.asej.2015.03.011.

APPENDIX

- PV: 200 kW, [Kyocera KC200GT]
- WTG: GAMESA G52/850, 850 kW, 690 V, 52 m, 2,124 m2, controlled-pitch; cut-in speed: 4 m/s, rated
- speed: 16 m/s, max. speed: 25 m/s, output speed of generator: 1900rpm
- 3 HHO: Iterations = 50, Hawks No. =25
- GA: population = 20, cross over = 0.85, mutation =0.08, and maximum no. of iterations = 100